ACS APPLIED MATERIALS & INTERFACES

Research Article

www.acsami.org

Three-Dimensional Homogeneous Ferrite-Carbon Aerogel: One Pot Fabrication and Enhanced Electro-Fenton Reactivity

Yujing Wang,[†] Guohua Zhao,*[,†,‡] Shouning Chai,[†] Hongying Zhao,[†,‡] and Yanbin Wang[†]

[†]Department of Chemistry and [‡]State Key Laboratory of Pollution Control and Resource Reuse, Tongji University, 1239 Siping Road, Shanghai 200092, PR China

Supporting Information

ABSTRACT: This work focuses on constructing a high catalytic activity cathode of an electro-Fenton system, to overcome the defects of low activity, poor stability, and intricate fabrication of supported catalysts. A series of ferrite-carbon aerogel (FCA) monoliths with different iron/carbon ratios was synthesized directly from metal−resin precursors accompanied by phase transformation. Self-doped ferrite nanocrystals and carbon matrix were formed synchronously via moderate condensation and sol-gel processes, leading to homogeneous texture. An optimal 5% ferric content FCA was composed of coin-like carbon nano-plate with continuous porous structure, and the ferric particles with diameters of dozens of nanometers were uniformly embedded into the carbon framework. The FCA exhibited good conductivity, high catalytic efficiency, and distinguished stability. When it was used as an electro-Fenton cathode, metalaxyl degradation results demonstrated that 98% TOC elimination was realized after 4 h, which was 1.5 times higher than that of the iron oxide supported electrode. It was attributed to self-doped Fe@Fe_2O_3 ensuring Fe(II) as the mediator, maintaining high activity via reversibe oxidation and reduction by electron transfer among iron species with different valences. Meanwhile, an abundance of independent reaction microspaces were provided for every ferric crystal to in situ decompose electrogenerated H_2O_2. Moreover, the possible catalytic mechanism was also proposed. The FCA was a promising candidate as potential cathode materials for high-performance electro-Fenton oxidation.

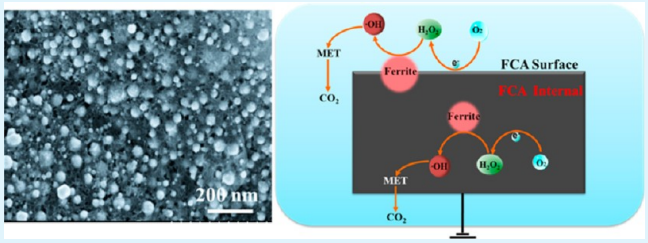

KEYWORDS: *Ferrite−carbon aerogel, monolith electrode, heterogeneous catalysis, metalaxyl, electro-Fenton, hydroxyl radical*

INTRODUCTION

Nowadays, a great development has been achieved for destructing persistent organic pollutants (POPs) in wastewaters by electrochemical advanced oxidation processes (EAOPs).[1−5] These eco-friendly methods are based on the in situ generation of hydroxyl radical (•OH). This species is the second strongest oxidizer known after fluorine and has a high standard redox potential (E^o(OH/H_2O) = 2.80 V/SHE), which can react with POPs non-selectively until their total mineralization (conversion into CO_2, water, and inorganic ions). Recently, the most common EAOP based on Fenton chemistry is the electro-Fenton (E-Fenton) process.[6] The E-Fenton system can continuously supply H_2O_2 through the two-electron reduction of active oxygen on the cathode (eq 1). Meanwhile, Fe^{2+} is added to react with H_2O_2 for producing •OH via homogeneous Fenton reactions (eq 2).[7−10] The above reaction is mainly propagated by the cathodic reduction of Fe^{3+} to Fe^{2+} from eq 3.

$$O_2 + 2H^+ + 2e^- \rightarrow H_2O_2 \quad (1)$$

$$Fe^{2+} + H_2O_2 \rightarrow Fe^{3+} + {}^{\bullet}OH + OH^- \quad (2)$$

$$Fe^{3+} + e^- \rightarrow Fe^{2+} \quad (3)$$

However, the homogeneous electro-Fenton requires an optimum pH < 3 circumstance, large amounts of Fe^{2+} (50−80 ppm) and the effluent must be neutralized after disposal which results in the generation of abundant sludge. So heterogeneous E-Fenton oxidation has become prevalent for wastewater purification, where soluble Fe^{2+} is replaced by Fe-containing solids without the need of low pH and iron sludge treatment, which is of considerable interest.[11−14]

Hitherto, researchers have developed various methods to obtain functionalized E-Fenton cathodic materials and discussed their applications for mineralizing pollutants from an aquatic environment. For example, pyrrhotite ($Fe_{1-x}S$) powder was adhered on the top of graphite sheeting by the silver conductive paste and used as the cathodic heterogeneous Fenton catalyst to degrade biorefractory organics in landfill leachate.[15] Zhang and co-workers used Fe@Fe_2O_3 nanowires as an iron reagent mixing with multiwall carbon nanotubes and fixed to tetrafluoroethylene (PTFE) as E-Fenton cathode for degradation of rhodamine B (RhB) at neutral pH.[16] More recently, activated carbon-supported nano-FeOOH (FeOOH/AC) was prepared by depositing iron oxide nanocrystals on the surface of activated carbon, and their E-Fenton oxidative behavior for amaranth was studied.[17] However, these function-

Received: October 23, 2012
Accepted: December 31, 2012
Published: December 31, 2012

alized E-Fenton cathodes were mainly formed by a supported or immobilized iron source on the conductive materials using multi-step preparation. Although the obtained electrodes achieved desirable reactivity, it was limited by the problems of catalyst fall off, dissolution, and agglomeration, resulting in catalyst activity decrease during the E-Fenton process. Moreover, the multistep method exposes the disadvantages of the complex preparation process and unevenly distributed catalysts, and the loss of the electrode body's catalytic role that resulted from the catalytic reaction only occurs at the electrode surface. To overcome these drawbacks, it is necessary to develop a more stable and efficient electrode material and convenient method for the heterogeneous E-Fenton system.

We notice that aerogel is a unique porous solid material with extremely low density (bulk densities 0.004-0.500 g/cm^3) that has open pores and high interior surface area. An overwhelming majority of the volume in an aerogel is air, which endows it with interesting physicochemical properties, such as the high porosity, being easily modified or functionalized, and excellent mass transfer.[18−20] For example, iron aerogel has been successfully prepared and applied in a catalytic Fischer-Tropsch reaction by Bali et al.[21] However, the pure iron aerogel mainly consists of Fe_3O_4, Fe_2O_3, and Fe_5C_2, which is unsuitable as an E-Fenton cathodic material due to its low conductivity, difficult electrogeneration of H_2O_2, and easily corrosion.

Herein, we are more interested in the hybrid aerogel which could well combine advantages of several materials to achieve special function. Carbon aerogel (CA) are characterized by high electrical conductivities and good corrosion resistance especially under the strongly oxidizing conditions;[22−25] meanwhile, iron aerogel possesses high mechanical robustness and thermal stability. Thus, a hybrid aerogel consisting of carbon and iron components could be envisioned as a prospective candidate for catalysis applications. It is our goal to obtain a highly uniform and stable cathode hybrid material for heterogeneous E-Fenton reaction by integrated iron aerogel and carbon aerogel.

Metalaxyl(*N*-methoxyacetyl-*N*-(2, 6-dimethylphenyl)-DL-alaninate, abbreviated to MET) is an active ingredient of conventional fungicides widely used in the control of plant diseases.[26] The formula is shown in Scheme 1. It is a chemically stable compound, resistant to a wide range of pH, temperature, and light. Large scale use of MET has been shown to affect the growth of soil microorganisms adversely. It has been reported that microbial mediated methods have been attempted to degrade it.[27] The Moza group has studied the degraded behavior under artificial sunlight.[26] But these methods do not yield its overall mineralization, that is, total conversion to CO_2, H_2O, and inorganic ions.

Scheme 1. Chemical Formula of Metalaxyl

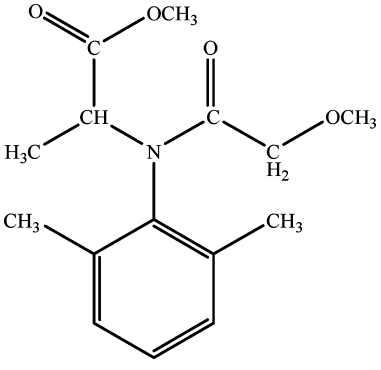

In the present work, we present a one-pot synthetic route for the fabrication of E-Fenton functionalized ferrite−carbon hybrid aerogels (FCA) using ferrous sulfate as a single iron precursor with simple heat treatment. The structure, morphology, property, and formation mechanism of the FCA are investigated. The catalytic activity is evaluated by degradation of MET. The proper mechanism for the great enhancement of FCA catalyst activity is analyzed in detail.

EXPERIMENTAL SECTION

Reagents and Materials. $FeSO_4·7H_2O$, Na_2CO_3, acetone, resorcinol, and formaldehyde were purchased from Sigma-Aldrich and used as received. All chemicals used in this study were of analytical grade. All solutions were prepared with deionized water.

Synthesis of FCA. The supercritical drying is a conventional method used for the preparation of an aerogel, but it requires reactors withstanding high pressure, which will greatly increase the manufacturing cost.[28,29] In this study, the ferrite−carbon aerogels electrode was prepared through sol-gel formation, solvent exchange, ambient pressure drying, and pyrolysis, according to a modified ambient drying technique.[23,30] Scheme 2 illustrates the preparation process of the FCA electrode. Firstly, resorcinol, formaldehyde, deionized water, and sodium carbonate are mixed with a molar ratio of 1:2:17.5:0.0008. After forming a homogeneous solution, a certain amount of ferrous sulfate solution is added dropwise to the precursor solution and then transfer into a cuboid glass with the interlayer distance of 5 mm. Secondly, the mixture is cured at 30 °C for one day, 50 °C for one day, and 90 °C to polymerize and age, resulting in metallic-organic wet gel and FCA former body, respectively. Thirdly, the as-prepared gel is immersed in acetone for 3 days in order to exchange the water in the former body and then dried under ambient conditions to obtain a massive dry gel with integrated structure. Finally, it is carbonized in a tubular oven by pyrolysis, which is kept at 950 °C for 4 h in argon atmosphere with the flow rate of 200 mL min^{-1}. A series of FCAs with different Fe content are obtained. For comparison, the carbon aerogels (CA) electrode was prepared by the same procedure above without $FeSO_4·7H_2O$ addition.

Characterization. The content of Fe in the synthesized samples was determined by inductively coupled plasma-optical emission spectroscopy (ICP-OES) technique, using a Thermo Scientific iCAP 6500 Duo ICP spectrometer. X-ray diffraction (XRD, Model D/max2550VB3+/PC, Rigaku) analysis was performed using a diffractometer with Cu Kα radiation, with an accelerating voltage of 40 kV and a beam current of 30 mA. Field-emission scanning electron microscopy (FE-SEM) and transmission electron microscopy (TEM) analysis were carried out, respectively, with a Hitachi S4800 and a JEM-2100, JEOL, with an accelerating voltage of 200 kV. The X-ray photoelectron spectra (XPS) were measured on an EScalab 250Xi spectrometer equipped with XR6 mononchromated X-ray source. The surface area and pore size of electrodes were measured by BET nitrogen adsorption at 77 K on a Micromeritics 3000 apparatus after heat treatment under vacuum at 573 K for 3 h. Thermogravimetric analysis (TGA) was carried out on a TG/DTA thermal analyzer (STA 409 PC Luxx, Netzsch Co. Ltd., Germany) with a heating rate of 10 °C min^{-1} in flowing N_2 atmosphere. Electrochemical performances were evaluated in a three-electrode cell system of a CHI 660C (CHI Co., USA) electrochemical workstation. A saturated calomel electrode (SCE) served as the reference and Pt foil as the counter electrode. Electrochemical impedance spectroscopy (EIS) was used to determine the conductivity of as-prepared electrodes, with the frequency range from 1×10^5 to 1×10^{-3} Hz and amplitude 5 mV, and the electrolyte was a 0.1 M Na_2SO_4 solution.

Degradation of Metalaxyl and Analysis. Degradation of metalaxyl by E-Fenton catalysis was performed in a cylindrical single-compartment cell. The reactor was externally connected to circulating water to keep the reaction at a constant temperature of 25

Scheme 2. Illustration for Fabrication of FCA Electrode

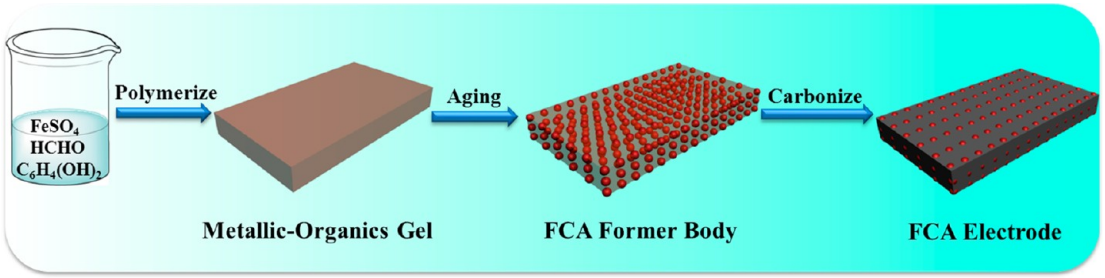

°C. The anode was a 4.5 cm^2 boron-doped diamond (BDD) thin film deposited on a single crystal Si sheet, with wide potential window and superior oxidation capability, which was purchased from CSEM (Switzerland). A cathode, FCA or CA with the same working area, was used, and the gap between the electrodes was 2 cm. High-purity oxygen was injected into the cell at 0.02 $m^3\ h^{-1}$ with a peristaltic pump. Constant current density of 10 mA cm^{-2} was applied in all systems except the single electrosorption (E-Adsorption) process, in which it was 0.5 mA cm^{-2}. Metalaxyl solution (100 mL, 500 mg L^{-1}) was degraded with 0.1 M Na_2SO_4 as the supporting electrolyte. In the comparative experiment of the homogeneous E-Fenton system, 1 mM L^{-1} Fe^{2+} was added as catalyst. The solution pH was measured with a Crison GLP 22 pH-meter and adjusted by 0.10 M NaOH or 0.10 M H_2SO_4 solution if needed.

Before analysis, all samples withdrawn from treated solutions were filtered with 0.45 μm PTFE filters. Total organic carbon (TOC) was measured on a Shimadzu TOC-Vcpn analyzer. The mineralization current efficiency (MCE) for electrolyzed solutions was calculated as follows[31]

$$\mathrm{MCE} = \frac{\Delta(\mathrm{TOC})_{\mathrm{exp}}}{\Delta(\mathrm{TOC})_{\mathrm{theor}}} \times 100\% \quad (4)$$

where $\Delta(\mathrm{TOC})_{\mathrm{exp}}$ is the experimental value for TOC removal at time t and $\Delta(\mathrm{TOC})_{\mathrm{theor}}$ is the theoretical value, calculated by

$$\Delta(\mathrm{TOC})_{\mathrm{theor}} = \frac{Itn_cM \times 10^3}{n_eFV}\ \mathrm{mg\ L^{-1}}$$

where I is the current intensity (A), t is electrolysis time (s), F is the Faraday constant (96485 C mol^{-1}), n_e is the electron transfer number in the mineralization reaction, n_c is the carbon number of the organic compound, M is carbon atomic weight (12 g mol^{-1}), and V is the volume of the sample solution (L). For metalaxyl, n_e and n_c are 78 and 15, assuming that its overall mineralization corresponds to the following reaction,

$$C_{15}H_{21}NO_4 + 29H_2O \rightarrow 15CO_2 + NO_3^- + 79H^+ + 78e^- \quad (5)$$

The concentration of metalaxyl in the E-Fenton oxidation process was analyzed by a reversed-phase high performance liquid chromatographer (HPLC, Agilent HP 1100, Agilent Corporation, USA) at room temperature equipped with an Agilent AQ-C18 column (4.6 mm ×150 mm ×5 μm) and selected photodiode detector at λ = 215 nm. The mobile phase was a mixture of methanol and water (70:30, v/v) with a flow rate of 1.0 mL min^{-1}.

The hydroxyl radicals were determined according to the literatures[32,33] in which formaldehyde was generated quantitatively by the reaction between hydroxyl radicals and dimethyl sulfoxide, and then reacted with 2,4-dinitrophenylhydrazine to form the corresponding hydrazone and analyzed by HPLC at room temperature with the same column mentioned above and with a selected UV detector at λ = 355 nm. The mobile phase was a mixture of methanol and water (60:40, v/v) at a flow rate of 1.0 mL min^{-1}. Specifically, the hydroxyl radicals generated on the cathode were determined in a divided system with 250 mM dimethyl sulfoxide.

The energy consumption (E_{TOC}) per unit TOC was calculated as follows:

$$E_{\mathrm{TOC}} = E_{\mathrm{electro}}/(\mathrm{TOC}_0 - \mathrm{TOC}_t) \quad (6)$$

$$E_{\mathrm{electro}} = UIt_{\mathrm{electro}} \quad (7)$$

where E_{TOC} was energy consumption per unit TOC removal (J per mg L^{-1} TOC), E_{electro} was total energy consumption of electrochemical reaction (J), and ($\mathrm{TOC}_0 - \mathrm{TOC}_t$) was the TOC removal (mg L^{-1}) in the t_{electro} time range. U was the cell voltage of electrochemical reaction (V), I was the current at this voltage (A), and t_{electro} was the time of reaction (s).

RESULTS AND DISCUSSION

Microstucture and Surface Properties of FCA. Carbon aerogel, which presents interconnected structure, high surface area, and good electrical conductivity, was derived from an organic sol–gel process, which is prepared by means of ambient drying technique. To expand the potential application in heterogeneous E-Fenton for these unique materials, we have focused on the impregnation of iron reagent into CA with the goal of modifying the structure, conductivity, and catalytic activity of the aerogel. Figure 1 shows the appearance of the

Figure 1. Photographs of CA and FCA's former bodies and final electrodes.

former body and final product of CA or FCA. With iron reagent incorporation, the appearance of the electrode is changed, and physical hardness increased obviously. When the iron content reaches 5%, the color of the FCA former body changes in appearance to red brown from the yellow of the CA, and the color of as-prepared FCA is black gray comparing to the black CA after heat treatment in N_2 atmosphere. The obtained FCA has a smooth surface and lack of obvious cracks, which ensures its good conductivity and high mechanical strength.

Apart from the approach of electrode preparation, one of the key factors of governing the oxidation performance of catalysts is the active component content. It has also been reported that

iron content influences both the textural characteristics of the composite and the catalytic ability.[34,35] The pure CA and a series of FCAs with different iron contents are prepared for studying the effect of iron addition on the CA morphology and physicochemical properties firstly. Figure 2 shows the representative SEM images of these as-prepared electrode materials. As shown in the Figure 2A, the CA without iron addition has loose network microstructure, and the porous structure is obviously observed. Through the impregnation of iron reagents into the initial organic precursor, the FCA can be readily obtained. It is seen that the morphology of FCA is similar to that of pure CA with a small amount of iron addition, and no apparent iron oxides appear in our experiment condition (Figure 2B,C). However, with the iron content increasing from 0.5 wt % to 2.5 wt %, the carbon substrate changes to more compact and uniform sponge-like inner microstructure and lots of iron oxide composite particles distribute evidently on the surface of the carbon matrix (Figure 2D). When the iron content reaches 5 wt %, the carbon framework of the FCA would be greatly modified not only in appearance but also in microstructure and morphology. It should be stressed that the physical hardness and mechanical strength of FCA increased remarkably even with a little iron species addition, while the bulk density changed slightly (Table 1). At the same time, the microscopic elementary unit of FCA becomes a coin-like carbon sheet with a diameter of about 5 μm and a thickness of about 100 nm (Figure 2E), which is possibly attributed to anisotropic growth directed by iron or iron oxide crystalline solid. In addition, it is noteworthy that a large amount of globular ferric nanoparticles embeds into a flaky carbon framework, and the whole network structure of FCA becomes more loose and multiporous, suggesting that the iron phase and carbon phase coexist well. It should be declared that, in our exploratory experiment, the FCA is too fragile to use as the electrode in the E-Fenton oxidation if the iron content is higher than or equal to 6 wt % (Table 1). This is possibly attributed to the excessive incorporation of iron that destroyed the cross-linking process of polymers. These features, to some extent, revealed that iron content of 5% would be the most suitable for gaining the stronger electrochemical capacity, higher exposure degree, and better dispersity of ferric crystals. Further degradation experiments also demonstrate that the Fenton catalytic activity of 5% iron ratio is the highest compared to those of other electrodes (detailed analysis is carried out in the following section). Therefore, we choose FCA electrodes with 5 wt % content as the focus of this study.

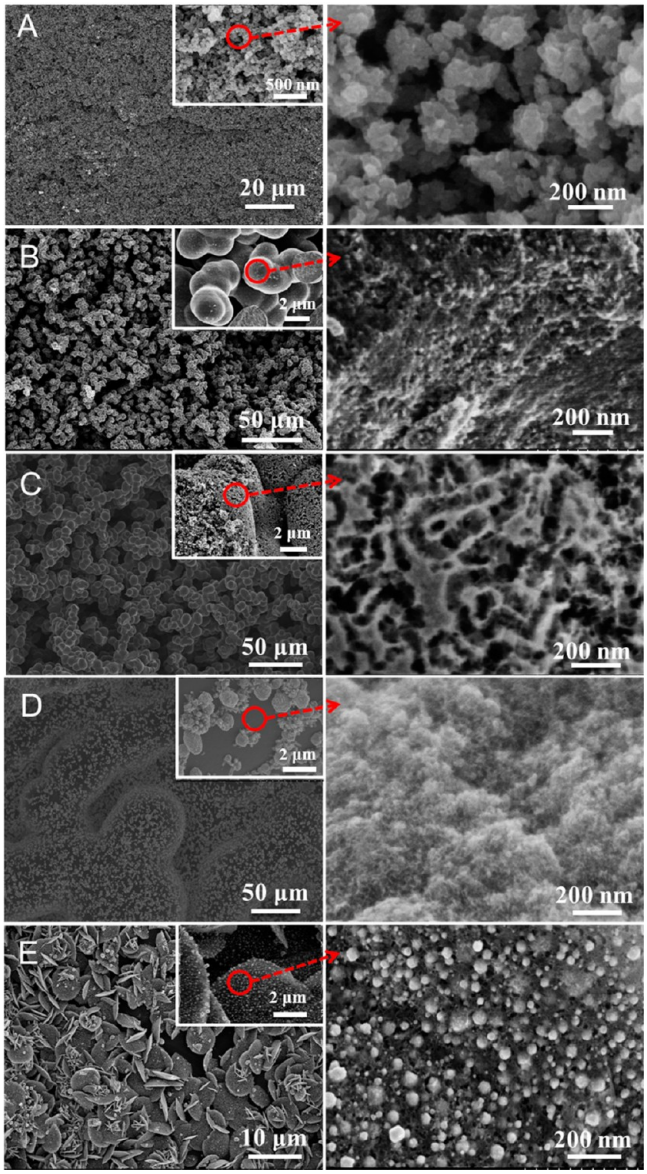

Figure 2. SEM images of CA and FCA electrodes with different iron contents: (A) pure CA, (B) 0.05 wt %, (C) 0.5 wt %, (D) 2.5 wt %, (E) 5 wt % .

TEM images of 5 wt % FCA (the abbreviation of FCA with 5 wt % iron content) in Figure 3 A,B clearly show that the size of the ferric nanoparticles is 80−120 nm, and these rough spherical nanoparticles are embedded in the carbon matrix just like plums in pudding. Such a geometric confinement of metal oxide nanospheres within carbon aerogel layers enhance efficiently their interfacial contact area with carbon matrix and suppress the dissolution and agglomeration of catalysts, thereby promoting the catalytic activity and stability of the hybrids.

Table 1. Comparison of Physico-Chemical Parameters of Several Electrodes

electrode materials	iron content (%)	S_{BET} (m^2/g)	micropore volume (cm^3/g)	bulk density (g/cm^3)	physical resistance (Ω)	appearance
graphite	0	5	0.00053	1.57	7.5	unbroken, black
CA	0	544	0.245	0.37	4.5	unbroken, black
FCA	0.05	490	0.202	0.37	8.0	unbroken, black
FCA	0.5	459	0.217	0.39	15.3	unbroken, gray black
FCA	2.5	449	0.199	0.51	25.0	unbroken, gray black
FCA	5.0	421	0.211	0.65	32.6	unbroken, black gray
FCA	6.0	413	0.205	0.67		crack, black gray

dx.doi.org/10.1021/am302437a | ACS Appl. Mater. Interfaces 2013, 5, 842−852

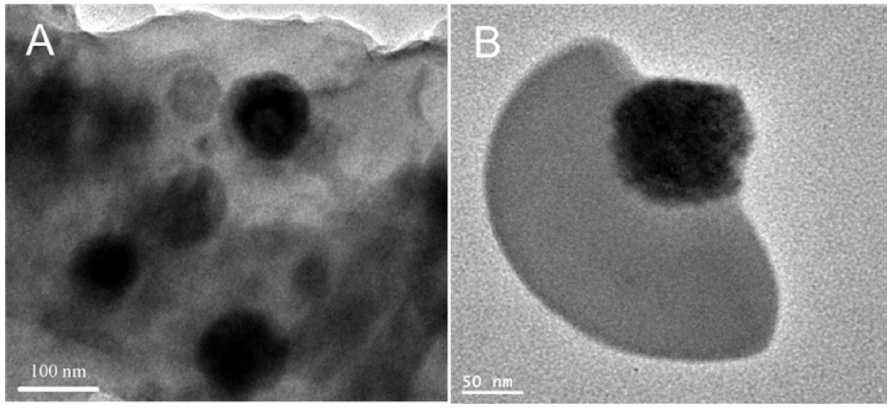

Figure 3. TEM images of 5 wt % FCA electrode.

To disclose the formation process of the electrode, XRD measurements of 5 wt % FCA calcined at different temperatures (200 °C, 500 °C, 600 °C, and 950 °C) are carried out, as shown in Figure 4A. It can be noticed that the two peaks at 2θ = 18.5° and 27.4° assigned to the $FeSO_4$ (JCPDS file No. 01-0703) are still obvious after 200 °C treatment, indicating that the decomposition of $FeSO_4$ does not yet occur. After 500 °C calcination, two small characteristic peaks of hematite (α-Fe_2O_3) appeare around 33.0° and 35.5°, corresponding to (104) and (110) planes (JCPDS file No. 33-0664), which reveals that the $FeSO_4$ has begun to decompose to the Fe_2O_3 at this temperature. When the calcined temperature increases to 600 °C, those two peaks become stronger and sharper; besides, several small peaks at 49.5°, 54.0°, 62.4°, and 64.0° newly emerge, which can be assigned to the (024), (116), (214), and (300) reflections of α-Fe_2O_3, a corundum crystalline structure. The appearance indicates that the crystallinity of α-Fe_2O_3 is better with 600 °C heat treating than that with 500 °C. The 5 wt % FCA with the 950 °C spectrum shows two broad peaks located at 2θ = 23.5° and 43.8°, attributed to the CA with noncrystalline structure, which is similar to the (002) and (101) facets of reflection of graphite (Figure 4B). Moreover, it can be seen in the XRD spectra that the two diffraction peaks of α-Fe_2O_3 became weaker, and a diffraction peak corresponding to the (110) plane of the metallic iron phase (JCPDS file No. 85-1410) due to carbon reduced the Fe_2O_3 to metal iron. Ultimately, the ferric substance is incorporated uniformly into the carbon aerogel framework in the obtained electrode in the coexistence form of α-Fe_2O_3 and zero valence iron.

The thermogravimetrics (TG) analysis further demonstrates the phase transformation of FCA in calcination. Figure 5 shows the TG and DTG results of the precursor (FCA former body which is without calcination) heat-treated under N_2 atmosphere. Three obvious valleys can be observed in the DTG curve. The first one below 200 °C is ascribed to the loss of water, and the other two are from the chemical reaction. The carbon precursor is deduced to start carbonizing at about 270 °C. Along with the calcination, the temperature is enhanced to 500 °C, and the reaction of $FeSO_4 = 0.5Fe_2O_3 + SO_2 + 0.25O_2$ (500−700 °C) occurs and Fe_2O_3 starts to generate. When the temperature is raised to 850 °C, metallic Fe is formed with the presence of reductive carbon at high temperature ($3C + 2Fe_2O_3 = 4Fe + 3CO_2$).

Generally, it is difficult to distinguish the magnetite (Fe_3O_4) and hematite (α-Fe_2O_3) from the XRD analysis only. Therefore, X-ray photoelectron spectroscopy (XPS) with high sensitivity to iron chemical state is used to study the compositions of the FCA.[36] Figure 6A demonstrates that elements of Fe, O, and C coexist in the as-prepared cathode. Figure 6B presents the high-resolution spectra of Fe 2p. The Fe 2p spectrum can be fitted into six peaks contribution at 706.8 eV, 710.7 eV, 713.6 eV, 719.0 eV, 720.0 eV, and 725.1 eV. The major contribution located at 710.7 eV and 725.1 eV are assigned to Fe $2p_{3/2}$ and Fe $2p_{1/2}$ of the lattice Fe^{III} in α-Fe_2O_3. According to the previous reported literatures,[37,38] the relatively weak contribution at 713.6.2 eV possibly belongs to the sulfide bonded iron (Fe^{II}−S), while contributions of binding energy at 706.8 and 720.0 eV are assigned to Fe $2p_{3/2}$ and Fe $2p_{1/2}$ of metal iron,[39] respectively. It has been reported that the Fe $2p_{3/2}$ level is characterized by the presence of a shake-up satellite at a binding energy of 719.0−719.8 eV for α-Fe_2O_3.[40−42] These satellites are frequently used as fingerprints to identify the iron oxide phases.[43] Herein, there is also a satellite peak appearance at 719.0 eV. Meanwhile, the O 1s spectrum of FCA is also recorded in Figure 6C which consists of two components. The first lower binding energy (~530.6 eV) component corresponds to the Fe−O bond in the Fe_2O_3. It has been reported that this component has a peak at the binding energy of 529.8−530.6 eV.[36,44,45] The second higher binding energy component corresponds to a binding energy of >532 eV, which should be attributed to chemisorbed oxygen, hydroxyl, or adsorbed water.[36,45] No O 1s peak assigned to SO_4^{2-} is found. The results demonstrated that $FeSO_4$ has decomposed completely, and Fe_2O_3 and zero valence iron are coexisting in the 5 wt % FCA at 950 °C calcination finally. Obviously, XPS patterns are in good agreement with the XRD data and reveal that the homogeneous bulk ferrite−carbon hybrid aerogel electrode is successfully obtained. The iron species is mainly composed of metal Fe and Fe_2O_3.

The N_2 adsorption−desorption isotherms and pore size distribution of the pure CA and FCA samples are depicted in Figure 7. The specific surface area of pure CA is 544 $m^2\ g^{-1}$. After incorporating 5.0 wt % iron reagent, the BET surface area remains at 421 $m^2\ g^{-1}$, presenting a relatively high value, which is essential for good electrosorption behavior to enrich the pollutants on the electrode. At the same time, the bulk density is obviously increased from 0.35 to 0.65 g cm^{-3} (Table 1), because a large amount of iron species is embedded in CA and part of it entered the carbon matrix in the sol−gel process. It should be noted that 5.0 wt % FCA has a porous characteristic and it is composed of both micropores and mesopores with sizes centered at 1.0 nm and 4.2 nm, respectively (inset of

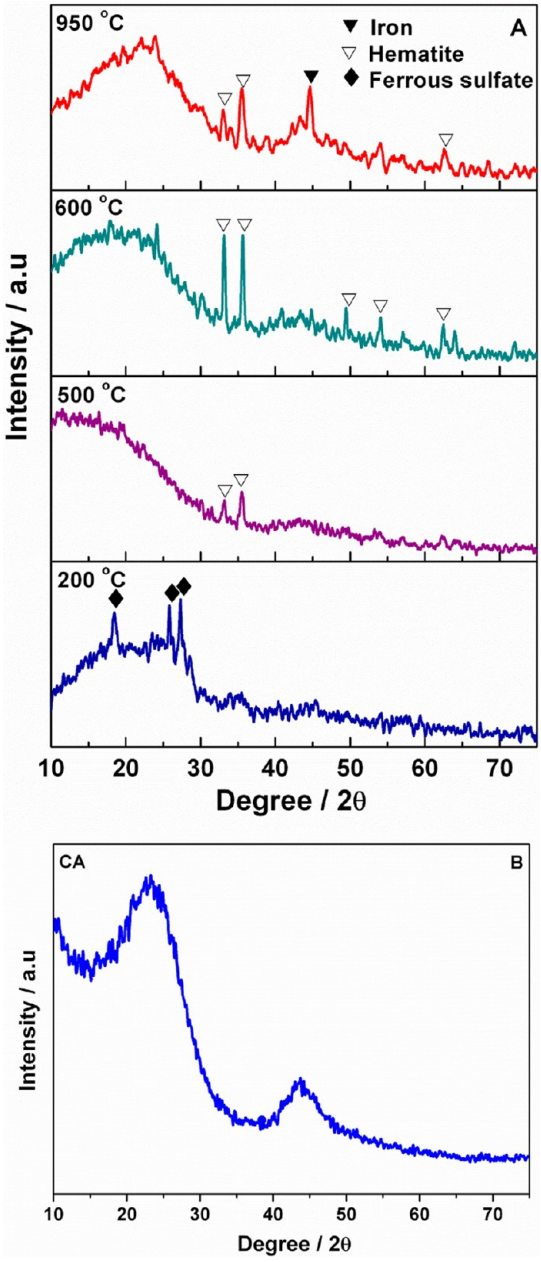

Figure 4. X-ray diffraction (XRD) patterns of 5 wt % FCA electrode calcined at different temperatures (A) and pure CA calcined at 950 °C (B) under N_2 atmosphere.

Figure 7). The catalytic behavior of 5.0 wt % FCA is closely related to not only the properties of iron reagent but also the porous texture of the substrates. Microporosity strongly favors the target pollutions adsorption capacity and tends to limit the metal leaching.[46,47]

Generally, an ideal E-Fenton electrode should not only have Fenton catalytic activity but also possess excellent electrochemical properties. Figure 8 shows the electrochemical impedance spectroscopy of pure CA and different FCA electrodes. The physical resistance of CA is 4.5 Ω (in Table 1), and the electrochemical impedance of CA is 3.8 Ω (shown in Figure 8). After iron reagent introduction, the values of the physical resistance and the electrochemical impedance are 32.6 Ω (in Table 1) and 78.5 Ω, respectively, indicating that the 5.0% FCA electrode still maintains good conductivity.

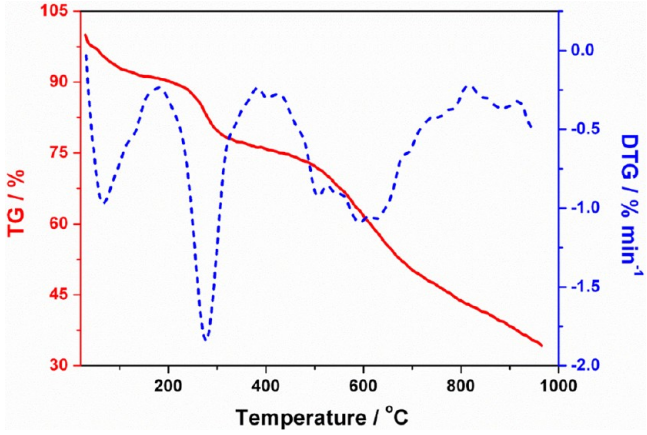

Figure 5. TG and DTG results of precursor of 5 wt % FCA electrode under N_2 atmosphere.

Furthermore, for the Nyquist plot of 2.5 wt % FCA, the semicircular loop at high frequency is relative small, and the slope of the impedance plot at the low frequency increases and tends to become purely capacitive, which may ascribe to its particular surface microstructure.

Application of FCA Cathode in E-Fenton Catalysis to Degrade Metalaxyl over Wide pH Range. To explore the catalytic activity of the obtained electrode with different iron content, we measure the •OH concentrations ($C_{\bullet OH}$) which are crucial parameters for manipulating the oxidation efficiency in the heterogeneous E-Fenton reaction. Figure 9A shows that the •OH radical is hardly to be produced on a traditional pure CA cathode, which results from the absence of iron reagent to decompose H_2O_2 generating •OH, while with FCAs as cathode, the values of $C_{\bullet OH}$ increase with iron reagent addition. $C_{\bullet OH}$ with 5 wt % FCA cathode is the highest among different electrodes. For example, at 120 min, $C_{\bullet OH}$ with 5 wt % FCA is 60.1 μM, which is 4 times that with 0.05 wt % FCA (15.0 μM). It suggests that 5 wt % FCA is a much more appropriate material in the E-Fenton process than other FCA electrodes. In 5 wt % FCA, abundant nano-sized iron species embedded in porous carbon with high exposure endows more catalytic active sites. When the H_2O_2 is electrogenerated via two-electron reduction reaction on 5 wt % FCA, it is decomposed promptly at the numerous nano-iron catalyst surfaces, which results in the •OH yield remarkably increasing. But in other FCA electrodes with lower content of iron, micrometer-sized iron particles attaching on the carbon surface (2.5 wt % FCA) decrease the reactive active area. With regard to the 0.05 and 0.5 wt % FCA, the armored carbon with iron core is possibly formed, limiting the catalytic activity due to low exposure of ferric catalyst.

The catalytic performance of optimized FCA is tested in different pH conditions. As shown in Figure 9B, it is interesting to find that the MET degradation efficiency keeps at a high level in a wide pH range from 3 to 9 in the heterogeneous E-Fenton process with 5 wt % FCA cathode. But in the traditional homogeneous E-Fenton system with free Fe^{2+} ion and CA cathode, the degradation rate of MET decreases rapidly as pH value increases. After 240 min, TOC removal remains at 98% at pH 6.0 in heterogeneous catalysis with 5.0 wt % FCA cathode, which is 1.4 times that in the homogeneous system. According to reports in the literatures,[48,49] the heterogeneous electro-Fenton reaction occurring on the surface of nano-iron catalyst can expand the working pH range. So the E-Fenton oxidation

dx.doi.org/10.1021/am302437a | ACS Appl. Mater. Interfaces 2013, 5, 842−852

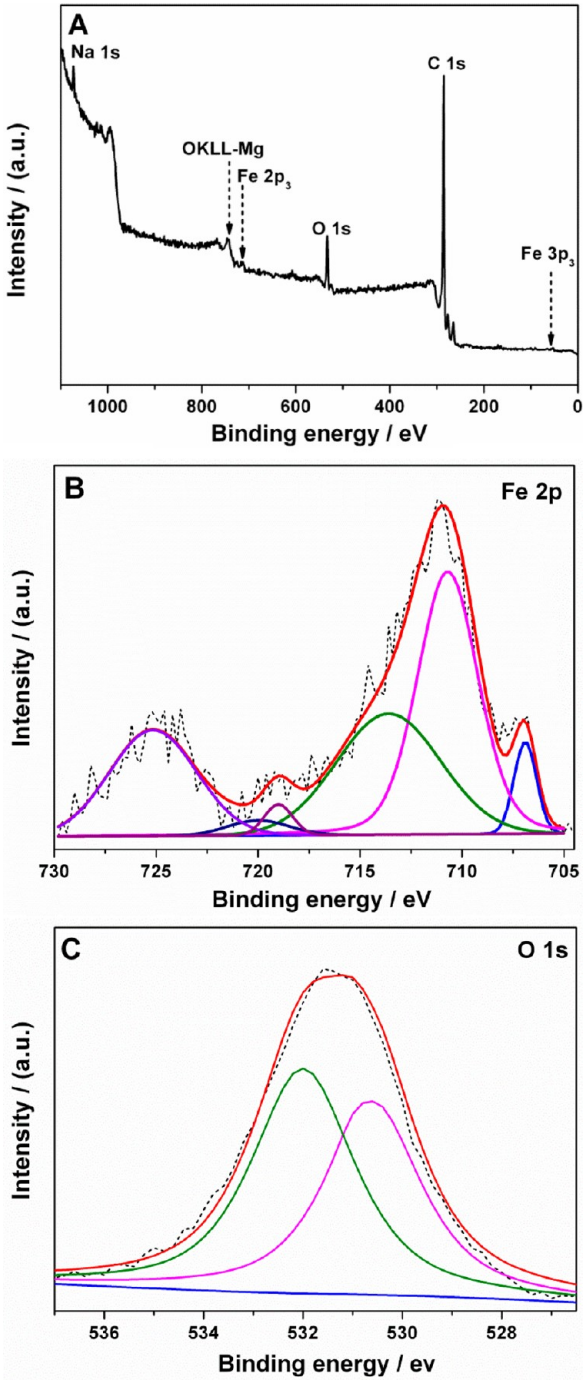

Figure 6. XPS spectra of the 5 wt % FCA: (A) survey of the sample, (B) Fe 2p, and (C) O 1s.

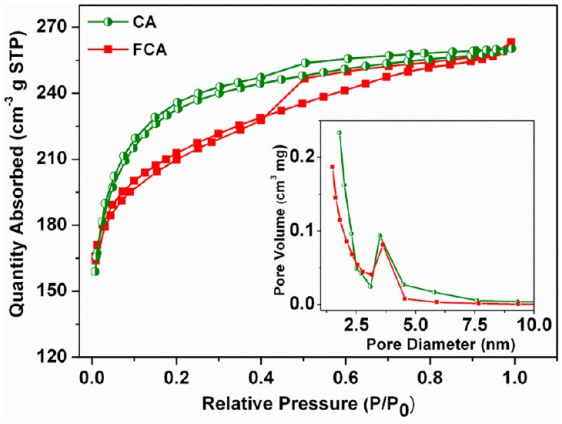

Figure 7. N_2 adsorption−desorption isotherms of CA and 5 wt % FCA electrode, and the corresponding pore size distribution is depicted in the inset plot.

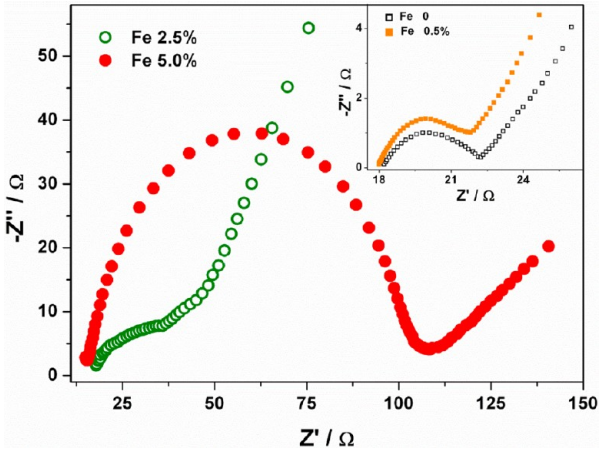

Figure 8. Electrochemical impedance spectroscopy of FCA electrodes with different iron content.

with FCA cathode mainly proceeds on the surface of nano-iron catalyst rather than resorting to dissolved Fe^{2+} as catalyst, which avoids the ferric ion precipitation effectively. The further catalysis mechanism of FCA is analyzed in the next section.

In order to study the effect of electrode morphology to catalytic ability, the commonly supported $Fe@Fe_2O_3/CA$ electrode is selected as a reference, whose morphology is shown in Figures S1 and S2 in Supporting Information. The E-Fenton oxidation efficiency with FCA cathode is evaluated by MET degradation at neutral pH. The TOC removal of MET is displayed in Figure 10A. In the solo E-Adsorption process with the FCA, 18% TOC removal is obtained at 240 min. It is due to the strong electrosorption capability of FCA. Although in an electrosorption process the applied potential is too low to trigger any electrochemical reaction, the pollutants are enriched on the surface of electrodes and keep a high local concentration by Coulomb interactions. So it would be very interesting to further study degradation efficiency based on this novel electrode in the E-Fenton oxidation process. It is noted that 5 wt % FCA exhibits superior removal efficiencies in the whole treatment stage compared to the supported electrode $Fe@Fe_2O_3/CA$. For example, 73% MET removal is reached at 60 min with 5 wt % FCA cathode, while the time required to reach the same value with supported $Fe@Fe_2O_3/CA$ is about 240 min. To study the catalytic performance to decompose H_2O_2 of 5 wt % FCA, a series of heterogeneous Fenton oxidations with adding a dose of H_2O_2 (5 mM) are performed, detailed in Supporting Information (Figure S3, S4, S5, and Text S1). During the E-Fenton oxidation process, numerous metalaxyl molecules are attacked by continuously generated $^{\bullet}OH$, and then produced various aromatic compounds such as 2,6-dimethylaniline, 2,6-dimethylacetanilide, and 2,6-dimethyl-*N*-ethylacetanilide at the initial stage as previously reported.[26] Then, those intermediates proceed consecutive hydroxylation steps and convert to a larger amount of polyphenolic and quinone substances. Simultaneously, the cleavage of some cyclic intermediates leads to formation of abundant small carboxylic

dx.doi.org/10.1021/am302437a | ACS Appl. Mater. Interfaces 2013, 5, 842−852

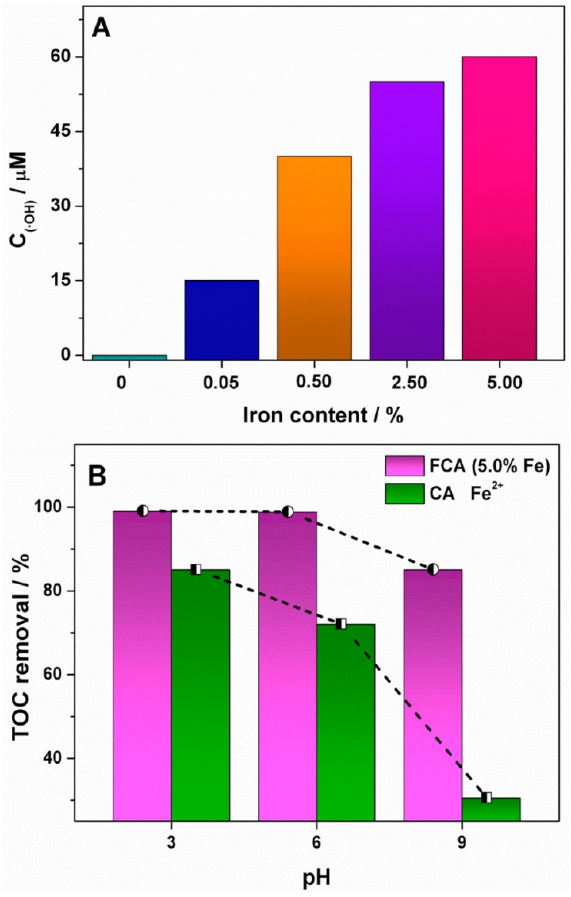

Figure 9. (A) Concentration of generated •OH with different iron content FCA electrodes in the E-Fenton system. (B) Effect of pH on TOC removal in homogeneous and heterogeneous E-Fenton systems.

acids including maleic acid, oxalic acid., etc. Finally, the metalaxyls are mineralized completely and TOC removal closes to 100% gradually along with an overwhelming majority of the aromatic and carboxylic acids by-products being oxidized to CO_2 and H_2O.

It is reconfirmed by the mineralization current efficiency (MCE) results as shown in Figure 10B. The efficiencies of the E-Fenton process with 5 wt % FCA, 2.5 wt % FCA, and Fe@Fe_2O_3/CA cathode are 73%, 61%, and 41% at 30 min, respectively. The results are consistent with TOC removal, further demonstrating that FCA is a suitable electrode in the E-Fenton system to generate more •OH for enhancing the efficiency of MET oxidation. Another parameter for evaluating the electrode is the energy consumption for removing the unit TOC in the degradation progress. The energy consumption with 5 wt % FCA electrode at 60 min is the lowest, 7.8 J per mg L^{-1} TOC, which is only 81% and 62% of that with 2.5 wt % FCA and Fe@Fe_2O_3/CA cathode, respectively, as shown in Figure 10C. It indicates that 5 wt % FCA not only presents excellent catalytic activity in the heterogeneous E-Fenton process but also possesses remarkable electrochemical properties for energy saving in wastewater treatment.

Since leached iron ions and recycling capability are crucial parameters for understanding the stability of the electrode, we measure the concentrations of Fe^{3+} and reusability of FCA in the heterogeneous E-Fenton system at neutral pH value, as respectively presented in Figure 11A,B. The leached iron ions of 5.0 wt % FCA are about 2% that of the supported Fe@

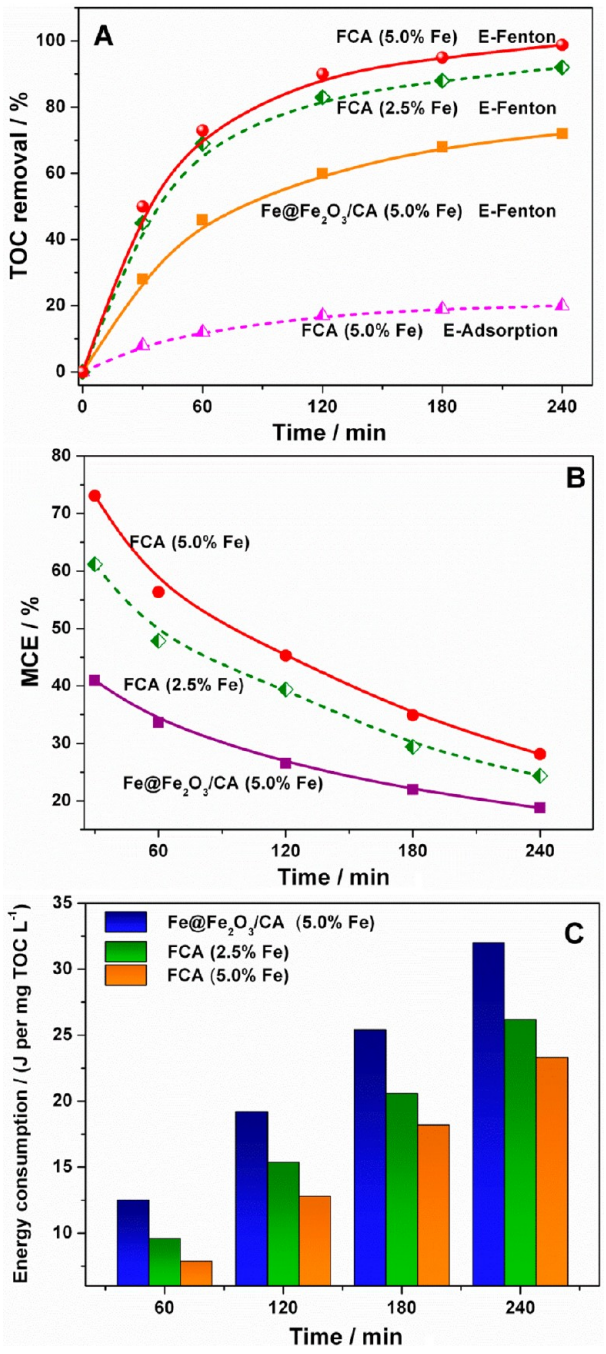

Figure 10. (A) TOC removal of MET with different cathodes; (B) mineralization current efficiency with different FCA cathodes in E-Fenton process; (C) energy consumption during E-Fenton process with different FCA cathodes.

Fe_2O_3/CA cathode during the whole E-Fenton process, indicating an almost completely surface-catalyzed process for H_2O_2 decomposition. To further demonstrate the stability of 5.0 wt % FCA material, we have analyzed the iron leached to the solution over time and characterized its microstructure after digesting in fixed pH 3.0 after 2400 min. The pH of 3.0 is known as the minimum value appropriate for the heterogeneous Fenton reaction. The concentration of leaching Fe^{3+} dependence time is determined (Figure S6, Supporting Information). Regarding the 5 wt % FCA, the concentration of leached Fe is very little, less than 0.8 mg L^{-1}. In addition, as

dx.doi.org/10.1021/am302437a | ACS Appl. Mater. Interfaces 2013, 5, 842−852

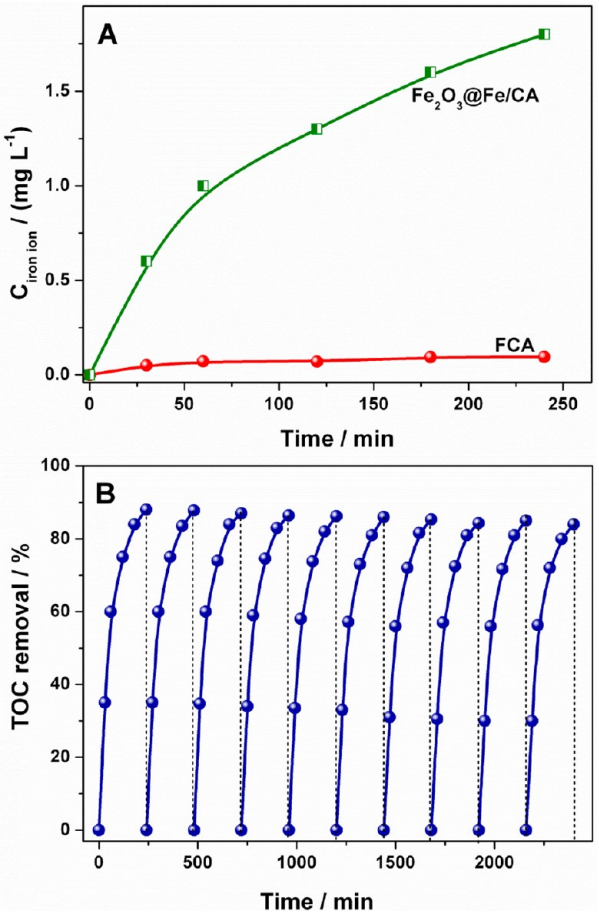

Figure 11. Stability of 5 wt % FCA cathode (pH = 6.0): (A) concentration of leached Fe^{3+} during E-Fenton process, (B) reusability of 5 wt % FCA.

shown in the TEM image with treated 5 wt % FCA (Figure S7, Supporting Information), the iron particles are also embedded in the carbon aerogel matrix clearly, and the diameter slightly reduces to about 65 nm from 80 nm of fresh samples due to small amounts of the Fe^{3+} leaching. The results confirm that the 5 wt % FCA is relatively stable even in acidic conditions within a certain period of time. Certainly, the stability will be much better in the neutral pH condition.

The stability of iron catalyst is generally related to the iron species, chemical state, crystallinity, surface physicochemical surroundings, and so on. In our work, the main active composition in FCA is α-Fe_2O_3. When the FCA is placed in the solution, it is known that the surface hydroxyl group may be formed by dissociative chemisorption of water molecules at exposed lattice metal ion sites on the α-Fe_2O_3 surface.[50] Compared with other iron oxide states, the α-Fe_2O_3 nanoparticles surface owned lower content of OH^- even at low pH (pH = 1–4), which could be explained by the cationic vacancies at surface sites of the corundum structure.[51] Thus the dissolution behavior is suppressed, and the catalyst keeps stability at a wide pH range. Moreover, the remarkable stability of the 5 wt % FCA electrode could also attribute that the inert carbon scaffold anchors every iron catalyst nanoparticle and the encapsulated structure effectively slows down the iron catalyst corrosion. Last but not least, from the XRD pattern, we can also observe that iron catalyst presents high cryastallinity, which may be another subordinate reason for the remarkable stability.

The recycling capability of the FCA electrode is evaluated by degrading MET over the reused cathode in the E-Fenton process (Figure 11B). The degradation efficiency does not notably decrease after 2000 min recycling utilization, suggesting that the FCA cathode is very stable and reusable in neutral pH.

Mechanism for Efficient Removal of MET with Novel FAC Cathode in E-Fenton Oxidation. According to the previous studies, the decomposition of H_2O_2 by mono/mixed solid iron oxides (e.g., goethite and hematite) generally includes two situations according to the different pH. Under low pH conditions, the process appears to be controlled by redox cycling of surface and dissolved iron (i.e., Fe[II]/Fe[III]), the latter resulting from dissolution of iron oxides.[48,52,53] At neutral pH value, the contribution of dissolved iron to H_2O_2 activation should be minimal because Fe(III) is indissolvable.[54,55] Therefore, the decomposition of H_2O_2 under neutral pH condition is considered as a surface-catalyzed process.

From the above analysis, the possible degradation process of MET in the E-Fenton process with FCA cathode at neutral pH is given in Scheme 3. At first, an abundance of active O_2 and

Scheme 3. MET Degradation Process in Heterogeneous E-Fenton System with FCA Cathode

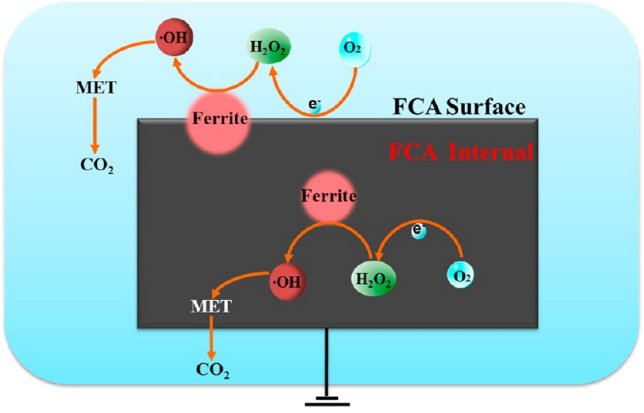

MET molecules are rapidly diffused toward the FCA surface and enriched in diverse size pores of FCA cathode under electrostatic interaction. Then, active O_2 capturing two electrons is reduced to H_2O_2 in situ on the interface between cathode and the water bulk phase (eq 1). Meanwhile, once H_2O_2 molecules are generated on the carbon matrix, it would be catalytically decomposed to strong oxidizer $^{\bullet}OH$ radicals by embedded iron oxide nanocrystalline promptly (eqs 9–12). The formed hydroxyl radical can then react by two different and competitive pathways: (i) the oxidation of organic pollutants and (ii) the reaction with H_2O_2 leading to the decomposition to O_2 via $HOO^{\bullet}$. Accordingly, the high-concentration contaminant accumulated on the electrode resulting from the electrosorption effect in situ capture $^{\bullet}OH$ radicals, preventing $^{\bullet}OH$ quenching and improving $^{\bullet}OH$ utilization. So the efficient mineralization to refractory pollutant MET is realized.

Although the kinetics of the E-Fenton process are very complex and depend on many different parameters, a critical step is certainly the production rate of $^{\bullet}OH$ from H_2O_2, which is generally correlated to the production of H_2O_2 and iron oxide properties.[56,57] So far, a consensus on the reaction mechanism does not exist, and it has been widely accepted that the heterogeneous E-Fenton catalysis presumably fits the

dx.doi.org/10.1021/am302437a | ACS Appl. Mater. Interfaces 2013, 5, 842–852

Haber–Weiss mechanism that is analogous to that observed in the homogeneous Fenton system. The surface-based mechanism is proposed as follows:

$$\equiv Fe^{III}—OH + e^- \rightarrow \equiv Fe^{II}—OH \quad (8)$$

$$\equiv Fe^{III}—OH + H_2O_2 \Leftrightarrow \equiv Fe^{III}—OH(H_2O_2)(s) \quad (9)$$

$$\equiv Fe^{III}—OH(H_2O_2)(s) \rightarrow \equiv Fe^{II}—OH(HO_2^{\bullet})(s) + H^+ \quad (10)$$

$$\equiv Fe^{II}—OH(HO_2^{\bullet})(s) \rightarrow \equiv Fe^{II}—OH + HO_2^{\bullet} + H^+ \quad (11)$$

$$\equiv Fe^{II}—OH + H_2O_2 \rightarrow \equiv Fe^{III}—OH + {}^{\bullet}OH + OH^- \quad (12)$$

$$HO_2^{\bullet} \Leftrightarrow H^+ + O_2^{\bullet -} \quad (13)$$

$${}^{\bullet}OH + MET \rightarrow CO_2 + H_2O \quad (14)$$

$$\equiv Fe^0 + 2\equiv Fe^{III} \rightarrow 3\equiv Fe^{III} \quad (15)$$

When negative potential applies on the FCA cathode, accompanied with large amounts of H_2O_2 generation, partial $\equiv Fe^{III}—OH$ on the Fe_2O_3 crystal surface reduces to $\equiv Fe^{II}—OH$ via obtaining an electron (eqs 1and 8). As presented in eq 9, in neutral pH, the catalytic reactions are initiated by the production of a precursor surface complex of H_2O_2, $\equiv Fe^{III}—OH(H_2O_2)_s$ represents the surface species of hydrogen peroxide, electrogenerating on the inner- or outer-carbon matrix. The surface H_2O_2 complex may further undergo a reversible ground-state electron transfer from the ligand to the central atom (eq 10), and then the successor complex would be activated to Fe(II) through eq 11. Accordingly, H_2O_2 is decomposed directly through Fe(II) catalysis to generate $^{\bullet}OH$ radicals (eq 12). Finally, the organic pollutants are mineralized to CO_2 and H_2O through $^{\bullet}OH$ attacking (eq 14). It is known that the formation rate of $^{\bullet}OH$ via Fenton reaction catalyzed by Fe^{2+} (76 $(mol/L)^{-1}$ s^{-1}) is 104–105 times faster than the Fe^{3+} catalyzed Fenton-like reaction [0.001–0.07 $(mol/L)^{-1}$ s^{-1}]. Voinov et al. reported[58] that the surface catalytic centers of Fe on iron oxide nanoparticles were at least 50-fold more effective for $^{\bullet}OH$ production than the dissolved Fe^{3+} ions at neutral pH. Therefore, this step of reduction of Fe(III) to Fe(II) is the rate-limiting step in the whole heterogeneous electro-Fenton reaction. In addition, the Fe oxidation state on the nanosurface plays a critical role in $^{\bullet}OH$ generation. Recently, it was found that a composite, enclosing zero valent iron with iron oxides, had higher reactivity in the oxidation of pollutants than zero valent iron or iron oxides alone due to the Fe_{surf}^{2+} species formed by electron transfer from Fe^0 to Fe^{3+} in the internal crystal at the interface metal/oxide and increasing of oxygen vacancies.[59,60] With regard to porous FCA, the active component is also the mixed phase of Fe with α-Fe_2O_3, which ensures Fe(II) as the mediator maintaining high catalytic activity via reversible redox by electron transfer among iron species with different valences (eq 15), and so exhibits distinguished catalytic ability to metalaxyl.

Carbon aerogel does not catalyze the decomposition of H_2O_2. Thus, the significant enhancement in H_2O_2 activation and decontaminate ability by 5 wt % FCA at circumneutral pH values compared to supported $Fe@Fe_2O_3$/CA cathode is attributable to the particular structure, iron oxidation state, and higher iron catalyst content. First, the porous structure and the impregnation of iron species within the carbon matrix might prevent the iron from aggregating into clusters and have better decentrality both on the surface and internally in the electrode. It results in improvement in the number and properties of the reactive surface sites to promote the $^{\bullet}OH$ radicals production. The role of steric position of reactive sites on redox processes has been deduced to be important in the reduction of carbon tetrachloride by Fe(II) associated with goethite, where the steric position of the latter can enhance multiple electron transfer reactions.[48,61] In a similar way, iron dispersion within the carhon matrix might favor those radical mechanisms above-mentioned, leading to more $^{\bullet}OH$ production during the decomposition of H_2O_2. Second, the higher efficacy of FCA compared with the supported cathode may also arise from the differences in electrostatic interaction and electrosorption capability to reagents (O_2, H_2O_2, metalaxyl, etc.) on the electrode surface, and loaded $Fe@Fe_2O_3$ may diminish the CA adsorption ability. Last but not least, based on the embedded structure, independent reaction spaces are provided for every nano-iron species to in situ catalytic decomposition of H_2O_2 while it was produced on the surrounding carbon, and numerous organic pollutants adsorbed onto the carbon framework are oxidized by those $^{\bullet}OH$ subsequently. Compared to loaded catalyst, the relatively isolated micro-architecture effectively anchors the E-Fenton catalysts in the sponge-like carbon as an integrated cathode, not only avoiding the waste and shedding of iron species in the reaction process but also increasing the stability of the catalyst.

CONCLUSIONS

In summary, the study reports a one-pot synthetic route for the fabrication of E-Fenton functionalized ferrite–carbon hybrid aerogels with simple heat treatment. In order to obtain fine dispersion of iron species on a carbon matrix and high Fenton catalytic activity, the effect of the iron/carbon ratio is evaluated. The results reveal that uniform spherical composite iron oxide nanoparticles are homo-dispersed into a carbon aerogel matrix with 3D embedded structure with optimum proportion of 5 wt % iron species. Accordingly, a new E-Fenton system with this novel bulk ferrite carbon hybrid aerogel is first established working at a wide pH range. Compared to the supported iron oxide electrode, the as-prepared material shows good E-Fenton catalytic activity after prolonged cycling. In 240 min, the TOC removal with the 5 wt % FCA cathode is 98%, 1.5 times that with supported iron oxide electrode. Inspired by the wonderful intrinsic properties and the easy fabrication procedure, the carbon hybrid aerogels could be promising candidates as potential cathodic materials for high-performance E-Fenton oxidation.

ASSOCIATED CONTENT

Supporting Information

Additional details and figures. This material is available free of charge via the Internet at http://pubs.acs.org.

AUTHOR INFORMATION

Corresponding Author

*Phone: (86)-21-65988570. Fax: (86)-21-65982287. E-mail: g.zhao@tongji.edu.cn.

Notes

The authors declare no competing financial interest.

■ ACKNOWLEDGMENTS

This work was supported jointly by the National Natural Science Foundation of China (Project NO. 21077077, 21207101), Shanghai Municipal Education Commission and Shanghai Educational Development Foundation (Project No. 2011CG19), and the Program for Young Excellent Talents in Tongji University (Project No. 2010KJ063).

■ REFERENCES

(1) Gao, G.; Vecitis, C. D. *ACS Appl. Mater. Interfaces* **2012**, *4*, 1478−1489.
(2) deKrafft, K. E.; Wang, C.; Xie, Z.; Su, X.; Hinds, B. J.; Lin, W. *ACS Appl. Mater. Interfaces* **2012**, *4*, 608−613.
(3) Isarain-Chávez, E.; Garrido, J. A.; Rodríguez, R. M.; Centellas, F.; Arias, C.; Cabot, P. L.; Brillas, E. *J. Phys. Chem. A* **2011**, *115*, 1234−1242.
(4) Niu, J.; Lin, H.; Xu, J.; Wu, H.; Li, Y. *Environ. Sci. Technol.* **2012**, *46*, 10191−10198.
(5) Dirany, A.; Sirés, I.; Oturan, N.; Özcan, A.; Oturan, M. A. *Environ. Sci. Technol.* **2012**, *46*, 4074−4082.
(6) Brillas, E.; Sires, I.; Oturan, M. A. *Chem. Rev.* **2009**, *109*, 6570−6631.
(7) Garcia-Segura, S.; Garrido, J. A.; Rodriguez, R. M.; Cabot, P. L.; Centellas, F.; Arias, C.; Brillas, E. *Water Res.* **2012**, *46*, 2067−2076.
(8) Salazar, R.; Brillas, E.; Sires, I. *Appl. Catal., B* **2012**, *115*, 107−116.
(9) Almeida, L. C.; Garcia-Segura, S.; Arias, C.; Bocchi, N.; Brillas, E. *Chemosphere* **2012**, *89*, 751−758.
(10) Johnson, L. M.; DeForest, C. A.; Pendurti, A.; Anseth, K. S.; Bowman, C. N. *ACS Appl. Mater. Interfaces* **2010**, *2*, 1963−1972.
(11) Zhao, H.; Wang, Y.; Wang, Y.; Cao, T.; Zhao, G. *Appl. Catal., B* **2012**, *125*, 120−127.
(12) Dhakshinamoorthy, A.; Navalon, S.; Alvaro, M.; Garcia, H. *ChemSusChem* **2012**, *5*, 46−64.
(13) Navalon, S.; Dhakshinamoorthy, A.; Alvaro, M.; Garcia, H. *ChemSusChem* **2011**, *4*, 1712−1730.
(14) Navalon, S.; Martin, R.; Alvaro, M.; Garcia, H. *Angew. Chem., Int. Ed.* **2010**, *49*, 8403−8407.
(15) Li, Y.; Lu, A.; Ding, H.; Wang, X.; Wang, C.; Zeng, C.; Yan, Y. *Electrochem. Commun.* **2010**, *12*, 944−947.
(16) Ai, Z.; Mei, T.; Liu, J.; Li, J.; Jia, F.; Zhang, L.; Qiu, J. *J. Phys. Chem. C* **2007**, *111*, 14799−14803.
(17) Zhang, G.; Wang, S.; Yang, F. *J. Phys. Chem. C* **2012**, *116*, 3623−3634.
(18) Cabanas, A.; Enciso, E.; Carbajo, M. C.; Torralvo, M. J.; Pando, C.; Renuncio, J. A. R. *Chem. Mater.* **2005**, *17*, 6137−6145.
(19) Zou, J.; Liu, J.; Karakoti, A. S.; Kumar, A.; Joung, D.; Li, Q.; Khondaker, S. I.; Seal, S.; Zhai, L. *ACS Nano* **2010**, *4*, 7293−7302.
(20) Zhang, H.; Wang, C.; Wang, J.; Zhai, J.; Cai, W. *J. Phys. Chem. C* **2010**, *114*, 6446−6451.
(21) Bali, S.; Huggins, F. E.; Huffman, G. P.; Ernst, R. D.; Pugmire, R. J.; Eyring, E. M. *Energy Fuels* **2009**, *23*, 14−18.
(22) Worsley, M.; Satcher, J.; Baumann, T. *Langmuir* **2008**, *24*, 9763−9766.
(23) Wu, M.; Jin, Y.; Zhao, G.; Li, M.; Li, D. *Environ. Sci. Technol.* **2010**, *44*, 1780−1785.
(24) Paskevicius, M.; Tian, H.-Y.; Sheppard, D. A.; Webb, C. J.; Pitt, M. P.; Gray, E. M.; Kirby, N. M.; Buckley, C. E. *J. Phys. Chem. C* **2011**, *115*, 1757−1766.
(25) Biener, J.; Stadermann, M.; Suss, M.; Worsley, M. A.; Biener, M. M.; Rose, K. A.; Baumann, T. F. *Energy Environ. Sci.* **2011**, *4*, 656−667.
(26) Sukul, P.; Moza, P. N.; Hustert, K.; Kettrup, A. *J. Agric. Food. Chem.* **1992**, *40*, 2488−2492.
(27) Monkiedje, A.; Spiteller, M.; Bester, K. *Environ. Sci. Technol.* **2003**, *37*, 707−712.
(28) Horikawa, T.; Hayashi, J.; Muroyama, K. *Carbon* **2004**, *42*, 169−175.
(29) Wakayama, H.; Fukushima, Y. *Chem. Mater.* **2000**, *12*, 756−761.
(30) Jin, Y. N.; Zhao, G. H.; Wu, M. F.; Lei, Y. Z.; Li, M. F.; Jin, X. P. *J. Phys. Chem. C* **2011**, *115*, 9917−9925.
(31) Skoumal, M.; Arias, C.; Cabot, P. L.; Centellas, F.; Garrido, J. A.; Rodriguez, R. M.; Brillas, E. *Chemosphere* **2008**, *71*, 1718−1729.
(32) Tai, C.; Peng, J. F.; Liu, J. F.; Jiang, G. B.; Zou, H. *Anal. Chim. Acta* **2004**, *527*, 73−80.
(33) Gao, J. X.; Zhao, G. H.; Liu, M. C.; Li, D. M. *J. Phys. Chem. A* **2009**, *113*, 10466−10473.
(34) Wu, Z.; Yang, S.; Sun, Y.; Parvez, K.; Feng, X.; Muellen, K. *J. Am. Chem. Soc.* **2012**, *134*, 9082−9085.
(35) Jang, B.; Park, M.; Chae, O. B.; Park, S.; Kim, Y.; Oh, S. M.; Piao, Y.; Hyeon, T. *J. Am. Chem. Soc.* **2012**, *134*, 15010−5.
(36) Fujii, T.; de Groot, F. M. F.; Sawatzky, G. A.; Voogt, F. C.; Hibma, T.; Okada, K. *Phys. Rev. B* **1999**, *59*, 3195−3202.
(37) Guo, L.; Chen, F.; Fan, X.; Cai, W.; Zhang, J. *Appl. Catal., B* **2010**, *96*, 162−168.
(38) Han, W.; Gao, M. *Cryst. Growth Des.* **2008**, *8*, 1023−1030.
(39) Descostes, M.; Mercier, F.; Thromat, N.; Beaucaire, C.; Gautier-Soyer, M. *Appl. Surf. Sci.* **2000**, *165*, 288−302.
(40) Luo, M.; Bowden, D.; Brimblecombe, P. *Appl. Catal., B* **2009**, *85*, 201−206.
(41) Najjar, W.; Azabou, S.; Sayadi, S.; Ghorbel, A. *Appl. Catal., B* **2009**, *88*, 299−304.
(42) Karunakaran, C.; Anilkumar, P. *J. Mol. Catal. A: Chem.* **2007**, *265*, 153−158.
(43) Pariente, M. I.; Martínez, F.; Melero, J. A.; Botas, J. A.; Velegraki, T.; Xekoukoulotakis, N. P.; Mantzavinos, D. *Appl. Catal., B* **2008**, *85*, 24−32.
(44) Saleem, M.; Al-Kuhaili, M. F.; Durrani, S. M. A.; Bakhtiari, I. A. *Phys. Scr.* **2012**, *85*, 055802.
(45) Corneille, J. S.; He, J. W.; Goodman, D. W. *Surf. Sci.* **1995**, *338*, 211−224.
(46) Steiner, S. A., III; Baumann, T. F.; Kong, J.; Satcher, J. H., Jr.; Dresselhaus, M. S. *Langmuir* **2007**, *23*, 5161−5166.
(47) Zhou, Z.; Tian, N.; Li, J.; Broadwell, I.; Sun, S. *Chem. Soc. Rev.* **2011**, *40*, 4167−4185.
(48) Pham, A. L.; Lee, C.; Doyle, F.; Sedlak, D. *Environ. Sci. Technol.* **2009**, *43*, 8930−8935.
(49) Gonzalez-Olmos, R.; Martin, M. J.; Georgi, A.; Kopinke, F.-D.; Oller, I.; Malato, S. *Appl. Catal., B* **2012**, *125*, 51−58.
(50) Feng, J.; Hu, X.; Yue, P. L.; Zhu, H. Y.; Lu, G. Q. *Ind. Eng. Chem. Res.* **2003**, *42*, 2058−2066.
(51) Wang, C.; Baer, D. R.; Amonette, J. E.; Engelhard, M. H.; Antony, J.; Qiang, Y. *J. Am. Chem. Soc.* **2009**, *131*, 8824−8832.
(52) Pera-Titus, M.; Garcia-Molina, V.; Banos, M. A.; Gimenez, J.; Esplugas, S. *Appl. Catal., B* **2004**, *47*, 219−256.
(53) Kwan, W. P.; Voelker, B. M. *Environ. Sci. Technol.* **2002**, *36*, 1467−1476.
(54) Stefansson, A. *Environ. Sci. Technol.* **2007**, *41*, 6117−6123.
(55) Pham, A. L.-T.; Doyle, F. M.; Sedlak, D. L. *Environ. Sci. Technol.* **2012**, *46*, 1055−1062.
(56) Kwan, W. P.; Voelker, B. M. *Environ. Sci. Technol.* **2003**, *37*, 1150−1158.
(57) Petigara, B. R.; Blough, N. V.; Mignerey, A. C. *Environ. Sci. Technol.* **2002**, *36*, 639−645.
(58) Voinov, M. A.; Pagan, J. O. S.; Morrison, E.; Smirnova, T. I.; Smirnov, A. I. *J. Am. Chem. Soc.* **2011**, *133*, 35−41.
(59) Costa, R. C. C.; Moura, F. C. C.; Ardisson, J. D.; Fabris, J. D.; Lago, R. M. *Appl. Catal., B* **2008**, *83*, 131−139.
(60) Moura, F. C. C.; Oliveira, G. C.; Araujo, M. H.; Ardisson, J. D.; Macedo, W. A. A.; Lago, R. M. *Appl. Catal., A* **2006**, *307*, 195−204.
(61) Amonette, J. E.; Workman, D. J.; Kennedy, D. W.; Fruchter, J. S.; Gorby, Y. A. *Environ. Sci. Technol.* **2000**, *34*, 4606−4613.